Article

Cell

Post-translational Control of the Temporal Dynamics of Transcription Factor Activity Regulates Neurogenesis

Graphical Abstract

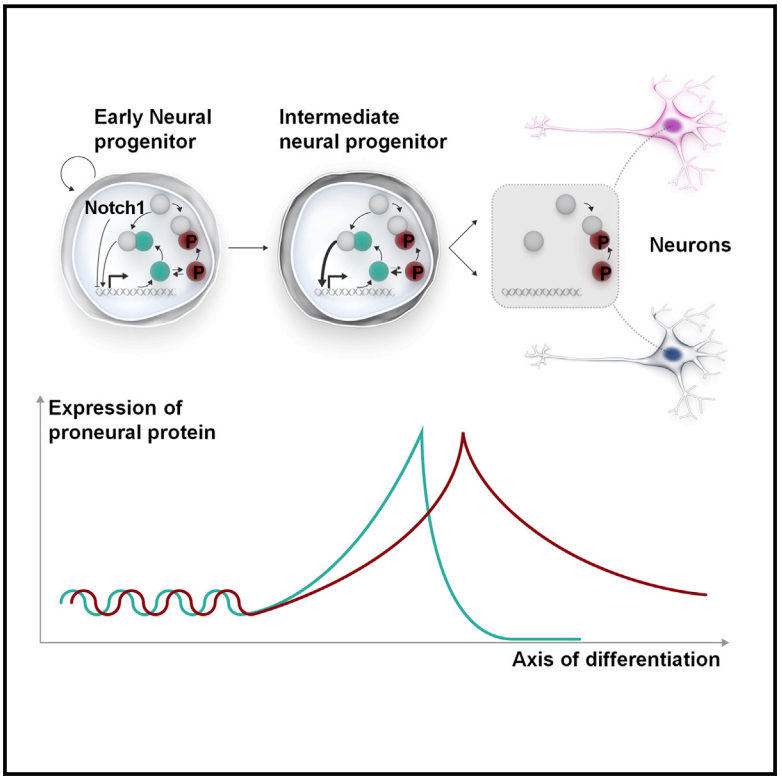

Authors

Xiao-Jiang Quan, Liqun Yuan, Luca Tiberi, ..., Huda Y. Zoghbi, Pierre Vanderhaeghen, Bassem A. Hassan

Correspondence

bassem.hassan@icm-institute.org

In Brief

The active lifetime of a family of transcription factors is regulated by phosphorylation, and even subtle changes to the timing of inactivation can disrupt the numbers and identities of neurons specified during development.

Highlights

- Proneural transcription factors driving neurogenesis show fast temporal dynamics
- A conserved phosphorylation site controls the temporal dynamics of these factors
- Inhibiting proneural phosphorylation alters the number of fate of nascent neurons
- Subtle quantitative interference with phosphorylation affects neuronal cell fate

Quan et al., 2016, Cell *164*, 460–475
January 28, 2016
http://dx.doi.org/10.1016/j.cell.2015.12.048

CellPress

Cell

Article

Post-translational Control of the Temporal Dynamics of Transcription Factor Activity Regulates Neurogenesis

Xiao-Jiang Quan,[1,2] Liqun Yuan,[1,2,3] Luca Tiberi,[4] Annelies Claeys,[1,2] Natalie De Geest,[1,2] Jiekun Yan,[1,2] Rob van der Kant,[5,6] Wei R. Xie,[7,8,9] Tiemo J. Klisch,[7,8,9] Joost Shymkowitz,[5,6] Frederic Rousseau,[5,6] Mathieu Bollen,[10] Monique Beullens,[10] Huda Y. Zoghbi,[7,8,9,11] Pierre Vanderhaeghen,[1,2,4] and Bassem A. Hassan[1,2,3,12,*]

[1]VIB Center for the Biology of Disease, VIB, 3000 Leuven, Belgium
[2]Center for Human Genetics, University of Leuven School of Medicine, 3000 Leuven, Belgium
[3]Program in Molecular and Developmental Genetics, Doctoral School for Biomedical Sciences, University of Leuven School Group Biomedicine, 3000 Leuven, Belgium
[4]Welbio, Université Libre de Bruxelles (ULB), Institute for Interdisciplinary Research (IRIBHM), and ULB Institute of Neuroscience (UNI), 1070 Brussels, Belgium
[5]VIB Switch Laboratory, 3000 Leuven, Belgium
[6]Department for Cellular and Molecular Medicine, University of Leuven School of Medicine, 3000 Leuven, Belgium
[7]Integrative Molecular and Biomedical Sciences Graduate Program, Baylor College of Medicine, Houston, TX 77030, USA
[8]Department of Molecular and Human Genetics, Baylor College of Medicine, Houston, TX 77030, USA
[9]Jan and Dan Duncan Neurological Research Institute at Texas Children's Hospital, Houston, TX 77030, USA
[10]Laboratory of Biosignaling and Therapeutics, Department of Cellular and Molecular Medicine, University of Leuven School of Medicine, 3000 Leuven, Belgium
[11]Howard Hughes Medical Institute, Baylor College of Medicine, Houston, TX 77030, USA
[12]Present address: Institut du Cerveau et de la Moelle épinière (ICM), 75013 Paris, France
*Correspondence: bassem.hassan@icm-institute.org
http://dx.doi.org/10.1016/j.cell.2015.12.048

SUMMARY

Neurogenesis is initiated by the transient expression of the highly conserved proneural proteins, bHLH transcriptional regulators. Here, we discover a conserved post-translational switch governing the duration of proneural protein activity that is required for proper neuronal development. Phosphorylation of a single Serine at the same position in Scute and Atonal proneural proteins governs the transition from active to inactive forms by regulating DNA binding. The equivalent Neurogenin2 Threonine also regulates DNA binding and proneural activity in the developing mammalian neocortex. Using genome editing in *Drosophila*, we show that Atonal outlives its mRNA but is inactivated by phosphorylation. Inhibiting the phosphorylation of the conserved proneural Serine causes quantitative changes in expression dynamics and target gene expression resulting in neuronal number and fate defects. Strikingly, even a subtle change from Serine to Threonine appears to shift the duration of Atonal activity in vivo, resulting in neuronal fate defects.

INTRODUCTION

The nervous systems of higher animals have an astonishing diversity of neurons. Yet, a small number of transcription factors are needed to generate and determine the identity of neurons. An even smaller subset called basic-Helix-Loop-Helix (bHLH) proneural proteins are the key initiators and regulators of generation of neurons from early neural progenitors (Bertrand et al., 2002; Hassan and Bellen, 2000). The *Drosophila* Achaete-Scute Complex (AS-C) genes are necessary and sufficient for the specification of peripheral nervous system (PNS) sensory organ precursors from neuroectodermal cells (Campuzano and Modolell, 1992; Ghysen and Dambly-Chaudiere, 1989; Jan and Jan, 1994), while the Atonal (Ato) protein (Jarman et al., 1993) is the proneural factor of the fly neural retina (Jarman et al., 1994, 1995). In the mammalian cortex and spinal cord bHLH proneural proteins such as Achaete-Scute homolog 1 (Ash1) and Neurogenin 2 (Ngn2) regulate the proneural transition (Casarosa et al., 1999; Fode et al., 1998; Ma et al., 1998). Mammalian Atonal homolog 1 (Atoh1/Math1) is required for the generation of granule neurons of the cerebellum from midbrain progenitors (Ben-Arie et al., 1997). A second homolog, Atoh7/Math5, is required for the formation of retinal ganglion cells from retinal progenitors (Brown et al., 1998; Wang et al., 2001). The conservation of Ato function across species is highlighted by the rescue of Atoh1-null mice by Ato (Wang et al., 2002). What remains unclear in all these systems is how the precise spatiotemporal pattern of proneural activity is regulated and how it contributes to neural specification. Furthermore, proneural proteins are expressed very transiently during early neurogenesis. How does a small set of proteins with a very short burst of expression underlie the generation of a large number and diversity of neurons? What are the causes and consequences of this short burst of

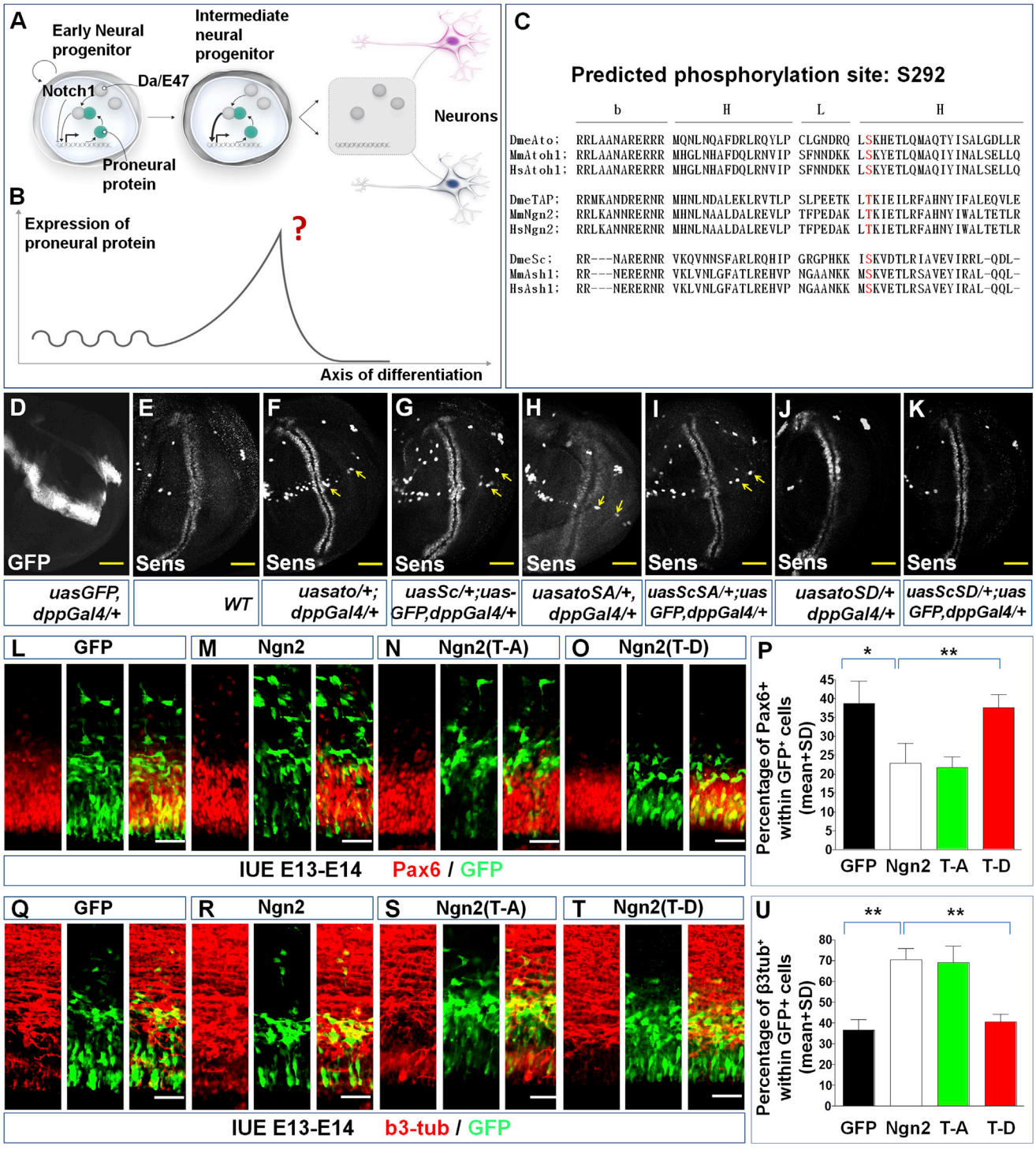

Figure 1. A Conserved Ser/Thr Residue Controls Proneural Activity

(A) Scheme of neural-fate transitions relative to proneural protein activity dynamics.

(B) Scheme of the expression dynamics of proneural proteins during neural-fate specification.

(C) Sequence of the proneural bHLH domain. The predicted Ser/Thr phosphorylation site is highlighted in red.

(D–K) Expression of Ato and Sc along in L3 wing discs with *dpp-Gal4*. (D) *dpp-Gal4* expression revealed by *UAS-GFP*. (E) Wild-type Sens expression in a few sensory organ precursors along the A-P margin. Expression of Ato (F) or Sc (G) induces ectopic Sens expression, as does expression of Ato^{SA} (H) and Sc^{SA} (I), but not Ato^{SD} (J) or Sc^{SD} (K).

(legend continued on next page)

expression? And finally, is there a general mechanism that applies to all nervous systems?

Studies in *Drosophila* and mouse have shown that the expression of proneural proteins begins at low levels in equivalent pluripotent progenitors and ramps up through auto-activation. Subsequently Notch-mediated lateral inhibition selects one of these progenitors to become a committed neural precursor that produces a diversity of neurons. This precursor elevates proneural gene expression first and then quickly extinguishes it. Thus, there are two general features of proneural protein activity: amplitude and duration. The increase in expression amplitude is easy to explain by auto-activation. However, amplitude increase places a constraint on duration. How does an auto-activating protein disappear at the peak of its expression? This suggests the existence of an unknown mechanism that overrides auto-activation and allows the synchronization of the amplitude and duration of expression. Conservation of the temporal sequence of proneural expression suggests an intrinsic feature common to all proneural proteins.

The *Drosophila* retina is a powerful system to dissect the quantitative control of proneural protein expression at high cellular and mechanistic resolution (Kumar, 2010; Quan et al., 2012; Rister et al., 2013). Neurogenesis in the retina begins when a wave of cell-fate specification (Wolff and Ready, 1991) sweeps across the developing eye primordium. The proneural protein Ato controls the switch from progenitors to photoreceptor neurons (Jarman et al., 1994, 1995). Both Ato protein and mRNA are thought to be transiently expressed in retinal progenitors and committed precursors. Subsequently, lateral inhibition selects a single precursor that differentiates into the first photoreceptor neuron called R8. The nascent R8 secretes the *Drosophila* Epidermal Growth Factor (EGF) Spitz, which activates the EGF Receptor (EGFR) in neighboring precursors transforming them into photoreceptor neurons (Freeman, 1994; Tio et al., 1994). Each R8 cell will eventually be surrounded by seven other neurons (R1–R7).

In the mouse cortex, neural progenitors give rise to a temporal sequence of neurons that migrate and arrange themselves in layers from deep to superficial. Early born neurons reside in the deep layers and express markers such as Tbr1, while late-born neurons inhabit more superficial layers and express markers such as Crux1. Like in *Drosophila*, the transition from neural progenitors to neurons is governed by the activity of proneural proteins, notably Ngn2 (Nieto et al., 2001).

We report the discovery of a deeply conserved Serine (Ser)/Threonine (Thr) residue within the bHLH domain of proneural proteins. The phosphorylation of this residue is a binary switch for the activity of all three proneural protein classes, Ato, Ngn, and Achaete-Scute (Ac-Sc). Using mouse and fly models, we show that phosphorylation of this residue inactivates proneural proteins. Structural modeling and biochemical analyses suggest that this is due to interference of the phospho-group with DNA binding. Genome editing of *Drosophila ato* shows that inhibiting the phosphorylation of the Ato Ser changes protein activity dynamics causing quantitative changes in the expression of target genes. This, in turn, interferes with signaling between nascent neurons with profound consequences for neuronal number and diversity. Strikingly, even a subtle change from Ser to Thr causes highly specific alterations in Ato dynamics and neuronal-fate specification. This work uncovers a conserved post-translational mechanism for regulating neurogenesis.

RESULTS

A Conserved Phosphorylation Site Regulates Proneural Activity

Proneural proteins engage in a positive feedback loop (Figure 1A), but their expression is kept in check in early neural progenitors by Notch-dependent lateral inhibition. According to current models once an intermediate progenitor is selected Notch repression is alleviated and proneural protein expression peaks due to auto-activation, only to rapidly disappear (Figures 1A and 1B). How the auto-activation loop is broken is unknown. Equally unclear is whether transient activity of proneural proteins is important for neurogenesis.

Because all proneural proteins show these activity dynamics, we reasoned that it is an intrinsic property of the proteins themselves. Proneural proteins only share significant homology within the bHLH domain and two motifs containing a few invariant residues appear to account for functional specificity (Quan et al., 2004). One motif contains a highly conserved putative phosphorylation Ser/Thr residue (Figure 1C), located at the junction of the loop domain and the second helix (L-H2 junction).

To test whether this residue can be phosphorylated, in vitro peptides containing the Ser/Thr residue for Ato, Atoh1, and Ngn2 were generated (Figures S1A–S1D) and tested against candidate Ser/Thr kinases. The sequence surrounding the Ser in the Ato and Ac-Sc group proteins resembles a moderate (Ato) or strong (Atoh1, Sc) PKA consensus sequence (NetPhos). All three peptides can be phosphorylated by PKA in vitro, but not when the Ser is replaced by Ala (Figures S1A–S1C). The Ngn2 sequence surrounding Thr 149 did not match known kinase consensus sequences. We screened 229 human commercially available Ser/Thr kinases and found that Ngn2 can be most significantly phosphorylated by MARK1 and PLK1 (Figure S1D).

To test whether the Ser/Thr residue regulates proneural activity in vivo, we generated both phospho-null (S/T > A) and phospho-mimetic (S/T > D) forms for one representative of each of the

(L–O) Coronal sections stained for GFP and Pax6 24 hr after in utero electroporation (E13.5–14.5) of pCIG (L), pCIG Ngn2-myc (M), pCIG Ngn2(TA)-myc (N), and pCIG Ngn2(TD)-myc (O).

(P) Quantification of cells stained for Pax6 among the GFP$^+$ cells. Mean ± SD, n = 6 embryos. Student's t test; *p < 0.05, **p < 0.01.

(Q–T) Coronal sections stained for GFP and β3-tubulin 24 hr after in utero electroporation (E13.5–14.5) of pCIG (Q), pCIG Ngn2-myc (R), pCIG Ngn2(TA)-myc (S), and pCIG Ngn2(TD)-myc (T).

(U) Quantification of cells stained for β3-tubulin among the GFP+ cells. Mean ± SD, n = 6 embryos. Scale bar in this figure represents 50 μm. Student's t test; *p < 0.05, **p < 0.01.

See also Figure S1.

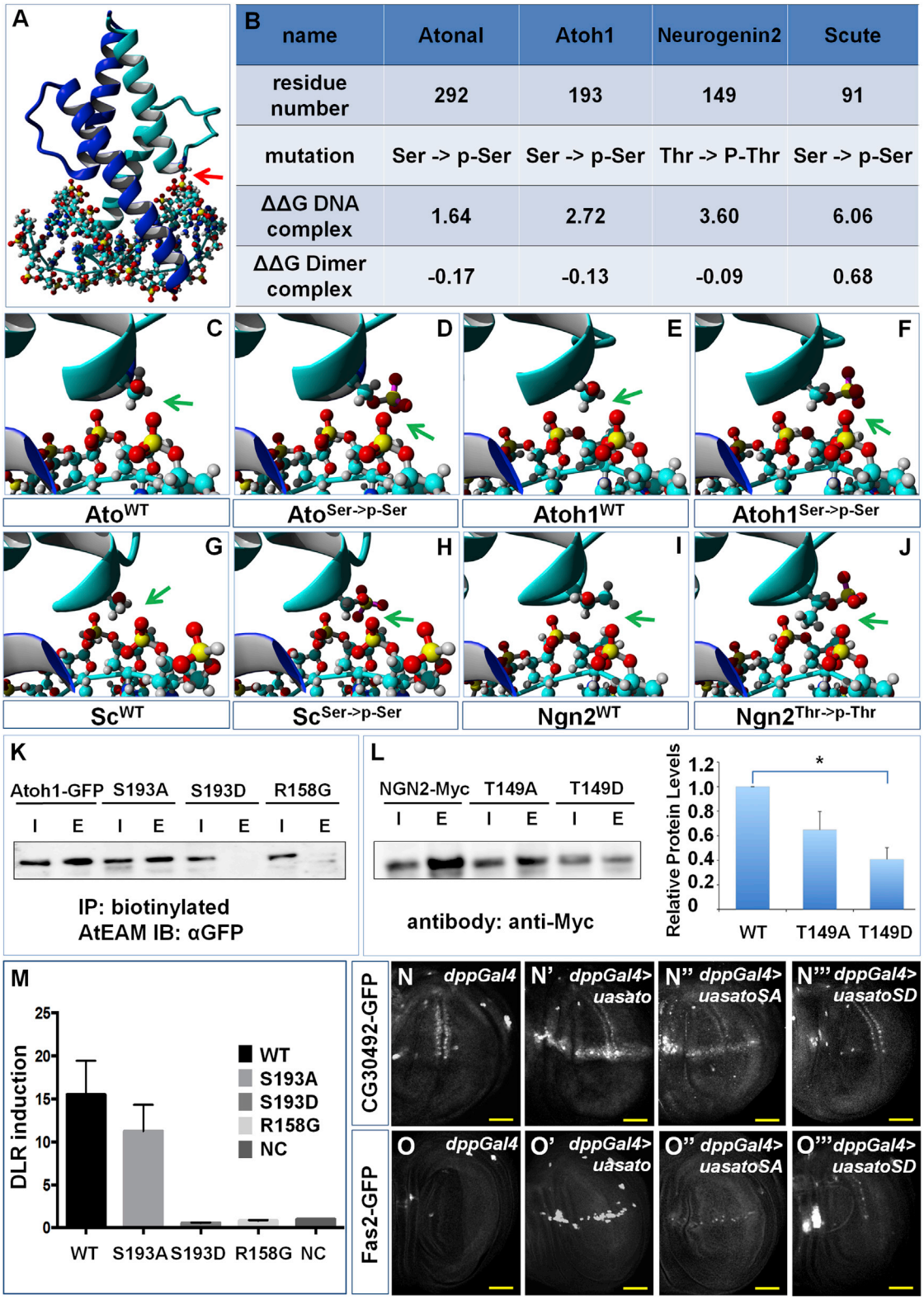

Figure 2. Phosphorylation of the Ser/Thr at the L-H2 Junction Controls DNA Interactions and Target Activation

(A) 3D model of DNA and proneural heterodimer complex. Arrow indicates the Ser/Thr.

(B) Theoretical energy required for ^{P}Ser/^{P}Thr to form DNA or protein heterodimer.

(legend continued on next page)

different proneural protein classes: *Drosophila* Scute (Sc) and Ato, and mouse Ngn2. These forms were tested in classical proneural assays in the developing *Drosophila* wing disc and the developing mouse cortex. All forms of Sc and Ato were transformed into the same genomic locus and multiple transformants tested. As positive controls, wild-type Sc (UAS-Sc) or Ato (UAS-Ato) were expressed along the anterior-posterior axis in the developing wing epithelium (using dpp-Gal4; Figure 1D) where very few neural precursors are normally specified (Figure 1E). This converts epithelial cells into neural precursors (Figures 1F and 1G) marked by the expression of Senseless (Sens; Nolo et al., 2001). Expression of Sc^{SA} and Ato^{SA} also converted epithelial cells into neural precursors (Figures 1H and 1I). In contrast, neither Sc^{SD} nor Ato^{SD} displayed proneural activity (Figures 1J and 1K).

Next, we tested the proneural activity of wild-type, phospho-null (T > A), and phospho-mimetic (T > D) forms of Ngn2 in the developing mouse cortex by in utero electroporation of GFP with the three different forms of Ngn2 (Figures 1L–1U). Wild-type Ngn2 converts radial glial progenitors into β3-tubulin positive neurons (Figures 1M and 1R). Expression of $Ngn2^{TA}$ results in quantitatively similar proneural activity to the wild-type protein (Figures 1N, 1S, 1P, and 1U). In contrast, $Ngn2^{TD}$ shows no significant proneural activity (Figures 1O, 1T, 1P, and 1U). Furthermore, neurons generated by wild-type and $Ngn2^{TA}$ show similar distributions in the cortical plate, while $Ngn2^{TD}$ shows a distribution pattern similar to GFP alone (Figure S1E).

The Proneural Phosphorylation Site Regulates Proneural Target Activation

How might phosphorylation of the proneural Ser/Thr residue located at the L-H2 junction regulate activity? While the basic domain of bHLH proteins is involved in DNA binding, the HLH domain is required for dimerization. We therefore tested the binding of the three forms of *Drosophila* Ato and mouse Atoh1 (wt, S > A, S > D) to Da and E47, respectively. Binding of Ato to Da was tested in a yeast two-hybrid assay, while binding of Atoh1 to E47 was tested by co-immunoprecipitation (coIP). We find that the wild-type, phospho-mimetic and phospho-null Ato and Atoh1 form heterodimers with Da/E47 (Figures S2A and S2B).

To gain insight into the potential causes of loss of proneural function we examined the position of the Ser/Thr residue in three-dimensional models of the Ato, Sc, Atoh1, and Ngn2 as heterodimers with Da (Sc, Ato) or E47 (Atoh1, Ngn2). Given the absence of atomic structures of these specific complexes, we resorted to constructing homology models using YASARA Structure (Krieger et al., 2002; Krieger and Vriend, 2002) in complex with DNA, using the structure of the heterodimer between E47 and SCL bound to DNA as a template (PDB: 2YPA, 2.80 Å; Table S1). These models show that the Ser/Thr residue is located within 10 Å of DNA particularly close to the negatively charged phosphate group in the DNA backbone (Figure 2A). Next, the effect of phosphorylation on the free energy of DNA binding by the heterodimers as well as the free energy of heterodimer formation was calculated using the FoldX force field (Schymkowitz et al., 2005). FoldX analysis predicted that phosphorylation destabilizes the complex with DNA but has no (for Ato, Atoh1, and Ngn2) or a minor (for Sc) negative effects on heterodimer formation (Figure 2B), using an error of 0.5 kcal/mol as a significance threshold in the FoldX calculations (>0.5 kcal/mol is destabilizing, < −0.5 kcal/mol is stabilizing). Phosphorylation results in the introduction of a negatively charged and relatively large moiety in close proximity of the DNA backbone phosphate (Figures 2C–2J), which is predicted to induce charge repulsion with DNA as well as Van der Waals clashes, destabilizing the complex between the DNA and the transcription factor by between 1.64 and 6.06 kcal/mol (Figure 2B). To test this prediction, we first carried out DNA pull-down assays using biotinylated DNA encoding proneural-specific E-boxes (Klisch et al., 2011) with different mutant forms of Atoh1 (wild-type $Atoh1^{WT}$, $Atoh1^{SA}$, $Atoh1^{SD}$, and the $Atoh1^{R158G}$ DNA binding mutant (Zhao et al., 2008). $Atoh1^{WT}$ and $Atoh1^{SA}$ bind DNA with equal efficiency. In contrast, the $Atoh1^{SD}$ mutant completely fails to do so, mimicking $Atoh1^{R158G}$ (Figure 2K). Similar experiments were carried out with $Ngn2^{WT}$ $Ngn2^{TA}$ and $Ngn2^{TD}$ (Figure 2L). $Ngn2^{TD}$ displayed significantly reduced, although not completely abolished, DNA binding activity compared to $Ngn2^{WT}$. There was no significant difference in binding between $Ngn2^{WT}$ and $Ngn2^{TA}$. To investigate the functional consequences of reduced DNA binding activity, we carried out enhancer-reporter assays in cell culture and flies. $Atoh1^{SD}$ shows significantly reduced transcriptional transactivation activity compared to wild-type or $Atoh1^{SA}$ in Luciferase reporter assay for transcriptional activity of the various Atoh1 proteins (Figure 2M). Transgenic flies with Ato target gene enhancers driving GFP reporters (CG30492-GFP and Fas2-GFP; Aerts et al., 2010) were examined upon overexpression of Ato^{WT}, Ato^{SA}, Ato^{SD} forms using dppGal4 (Figures 2N–2O′′′). Ato^{WT} (Figures 2N′ and 2O′) and Ato^{SA} (Figures 2N′′ and 2O′′) activated these reporters, while the Ato^{SD} failed to do so (Figures 2N′′′ and 2O′′′).

These observations suggest that phosphorylation of the proneural Ser/Thr residue is a binary switch for proneural protein function. To test this prediction and analyze its consequences

(C–J) Close view of Ser/Thr residue position (arrow) in various proneural protein 3D models. Ato^{WT} (C) and $Ato^{Ser- > P-Ser}$ (D), $Atoh1^{WT}$(E) and $Atoh1^{Ser- > P-Ser}$ (F), Sc^{WT}(G) and $Sc^{Ser- > P-Ser}$ (H), and $Ngn2^{WT}$(I) and $Ngn2^{Thr- > P-Thr}$ (J).

(K and L) In vitro DNA pull-down assay. Daoy cells transfected with either WT or mutant constructs of Atoh1-GFP or Ngn2-Myc. Cells were lysed 24 hr post-transfection and subject to immunoprecipitation with biotinylated DNA containing three Atoh1 E-Box Associated Motif (AtEAM) and agarose beads, followed by SDS-PAGE and immunoblotting with GFP or Myc antibody. Phospho-null proteins bind to the AtEAM, whereas phospho-mimetic proteins show a severe decrease in binding. R158G Atoh1, a DNA-binding mutant, is used as a negative control.

(M) Dual luciferase reporter (DLR) assay using a firefly reporter with a triple AtEAM and a minimal promoter. Transfection of wild-type (WT) Atoh1 activates the reporter by ~15-fold. S193A Atoh1 shows slightly decreased activation whereas S193D shows no activation ($p < 0.005$). Data are presented as mean ± SEM after normalization to negative control (NC; non-transfected). Scale bar, 50 μm.

(N–O′′′) Enhancer-reporter assays in *Drosophila*: UAS-Ato (N′ and O′), UAS-Ato^{SA} (N′′ and O′′), and UAS-Ato^{SD} (N′′′ and O′′′) using *dpp-Gal4*.

See also Figures S2A and S2B and Table S1.

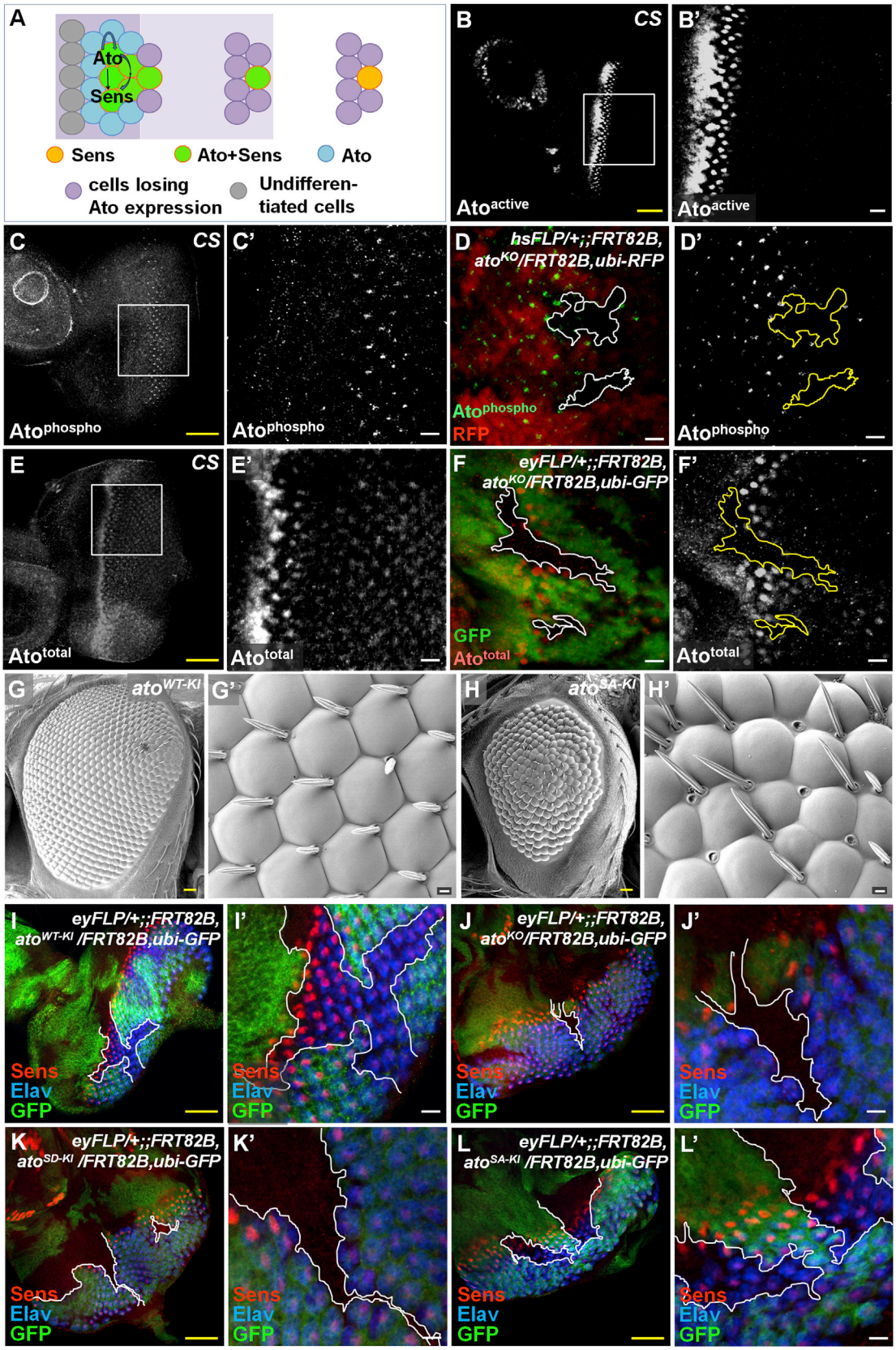

(legend on next page)

in vivo, we turned to the *Drosophila* retina and its proneural protein Ato as a model system.

Endogenous Atonal Is Phosphorylated on Ser 292 In Vivo

Available antibodies to Ato suggest that its expression is extinguished immediately upon selection of R8 photoreceptor neuron (Figures 3A–3B′). To test whether Ato is phosphorylated on the proneural Ser (S292 in Ato) in vivo, we generated a phospho-Ato-S292-specific monoclonal antibody (αAto^{phospho}) and carried out immunohistochemistry on third-instar larval (L3) eye discs. We find that αAto^{phospho} detects expression in the developing retina initially in a diffuse pattern in the morphogenetic furrow and then in R8 for a few rows (Figures 3C and 3C′), after Ato expression is reported to be extinguished. αAto^{phospho} is specific because it fails to detect signal in *ato* knockout clones (Figures 3D and 3D′; also see Figure 4 below). If Ato^{phospho} persists after R8 selection, why do existing antibodies not detect this form? We reasoned that phosphorylation interferes with these particular antibodies binding to Ato in vivo. We therefore tested a battery of guinea pig antibodies generated previously (Hassan et al., 2000) but never examined in the retina. One of these antibodies (GP49, renamed αAto^{total}) detects the entire pattern of Ato expression in wild-type, but not knockout tissue (Figures 3E–3F′). We therefore renamed the existing antibodies as αAto^{active} to denote that they detect the active but not the phosphorylated, putatively inactive, form of the protein.

Next, we sought to test whether Ngn2 is phosphorylated on the conserved Thr in cortical progenitors. IP of endogenous Ngn2 from E14.5 brain cortices showed that Ngn2 is recognized by a p-Thr antibody. Thus, Ngn2 is phosphorylated on one or more Thr residues in vivo (Figure S2C). To further test whether Ngn2-T149 is phosphorylated, we electroporated pCIG Ngn2^{WT}-myc and pCIG Ngn2^{TA}-myc in E13.5 embryos and performed Ngn2 IP 24 hr later using anti-myc antibodies. Ngn2^{WT} is recognized by the p-Thr antibody like endogenous Ngn2, while the mutant Ngn2^{TA} is barely detectable with the same antibody (Figure S2C). These data demonstrate that Ngn2-T149 is phosphorylated in vivo in cortical cells and suggest that T149 is either the only Thr phosphorylated in vivo or the seeding site of all other Thr phosphorylations. Next, we examined the phosphorylation of Ato by PKA in vivo. Compared to wild-type (Figures S2D and S2D′), misexpression of constitutively active PKA by *ey-Gal4* resulted in an increase of Ato^{phospho} (Figures S2E and S2E′) anterior to and in the morphogenetic furrow, where this signal is normally low. In contrast, misexpression of the PKA inhibitor, PKI, by *elav-Gal4* reduced the phosphorylation of endogenous Ato in the posterior aspects of the eye disc where the signal is normally stronger (Figures S2F and S2F′). In summary, both Ato and Ngn2 are phosphorylated in vivo. Next, we tested the consequences of interfering with Ato phosphorylation in vivo.

Phosphorylation Is a Binary Switch for Proneural Activity

To investigate the role of the conserved Ser in Ato activity dynamics and the consequences for neural specification, we replaced the endogenous *ato* locus with Ser-to-Ala (*ato*$^{SA\text{-}KI}$) and Ser-to-Asp (*ato*$^{SD\text{-}KI}$) mutations using the IMAGO (Choi et al., 2009) technique (Figure S3A). As a positive control, the endogenous *ato* coding sequence was replaced with wild-type *ato* (*ato*$^{WT\text{-}KI}$). As a negative control (*ato* knockout), we used the knockin of a *mini-white* marker (*ato*^{KO}). Similar to *ato*^{KO}, *ato*$^{SD\text{-}KI}$ animals are largely lethal during larval and pupal development (Figure S3B), suggesting that *ato*$^{SD\text{-}KI}$ is a null allele. In contrast, *ato*$^{SA\text{-}KI}$ flies develop to adulthood but show smaller eyes and disorganized facets (Figures 3G–3H′). Next, we generated clones for these alleles in the L3 eye disc. *ato*$^{WT\text{-}KI}$ clones are normal and generate R8 precursors (Sens^{+}) and differentiated neurons (Elav^{+}) in a wild-type pattern (Figures 3I and 3I′), while *ato*^{KO} clones and *ato*$^{SD\text{-}KI}$ clones fail to do so (Figures 3J–3K′). Next, we examined the effects of disabling S292 phosphorylation using the *ato*$^{SA\text{-}KI}$ flies. *ato*$^{SA\text{-}KI}$ clones do generate a single R8 and Elav positive cells (Figures 3L and 3L′) indicating that *ato*$^{SA\text{-}KI}$ encodes an active protein. Similar results were obtained for Sc whose loss of function in the fly scutellum was significantly rescued by Sc^{WT} and Sc^{SA}, but not Sc^{SD} (Figures S3C–S3I). Furthermore, *ato*$^{SD\text{-}KI}$ and *ato*^{KO} fail to activate known target enhancers, in contrast to *ato*$^{WT\text{-}KI}$ and *ato*$^{SA\text{-}KI}$ (Table S2; Figure S4). Thus, a phospho-mimetic form of Ato is a strong loss of function allele.

Loss of Phosphorylation Quantitatively Alters Proneural Isoform Balance

Next, we examined Ato expression and neuronal differentiation in *ato*$^{SA\text{-}KI}$ retina in greater detail using αAto^{phospho} and αAto^{active} antibodies. As opposed to the rapid loss of Ato^{active} expression upon R8 precursor selection in controls (Figures 4A–4A‴), Ato^{active} persists in *ato*$^{SA\text{-}KI}$ retina (Figures 4B–4B‴). In contrast, αAto^{phospho} fails to detect any signal in these eye discs (Figures 4C and 4C′) confirming the specificity of the antibody. *ato*$^{SA\text{-}KI}$/*ato*$^{WT\text{-}KI}$ eye discs show aberrant co-expression of Ato^{phospho} and Ato^{active} posterior to the morphogenetic furrow (Figures 4D and 4E). The low-level perdurance of Ato^{active} protein in *ato*$^{SA\text{-}KI}$ discs is not accompanied by a significant perdurance of the *Ato*

Figure 3. The Proneural Ser on Ato Is Endogenously Phosphorylated and Controls Activity

(A) Scheme of *Drosophila* R8 photoreceptor specification.

(B and B′) Expression of Ato^{active} in wild-type eye discs.

(C and C′) Ser 292 phosphorylated Ato in wild-type L3 eye disc revealed by the αAto^{phospho} antibody. Ato^{phospho} is weakly expressed in the MF and becomes stronger in the selected R8 for several rows.

(D and D′) αAto^{phospho} staining in L3 eye discs showing the lack of signal in *ato*^{KO} mutant clones (absence of RFP).

(E–F′) αAto^{total} staining of wild-type L3 eye disc (E and E′) and *ato*^{KO} mutant clones (absence of GFP; F and F′).

(G–H′) SEM images of the adult eyes of *ato*$^{WT\text{-}KI}$ (G) and *ato*$^{SA\text{-}KI}$ flies (H). (G′ and H′) High magnification of eyes in (G) and (H).

(I–L′) Clonal analysis of proneural activity for photoreceptor neuron formation in various Ato knockin mutants. Lack of GFP indicates the mutant clone. Sens (R8) and Elav (pan-R) mark differentiating photoreceptors. Positive control clones of *ato*$^{WT\text{-}KI}$ (I and I′). Negative control clones of *ato*^{KO} (J and J′). Clones of *ato*$^{SD\text{-}KI}$ (K and K′). Clones of *ato*$^{SA\text{-}KI}$(L and L′).

Scale bars, 50 μm in yellow and 10 μm in white. See also Figures S2C–S2F′, S3, and S4 and Table S2.

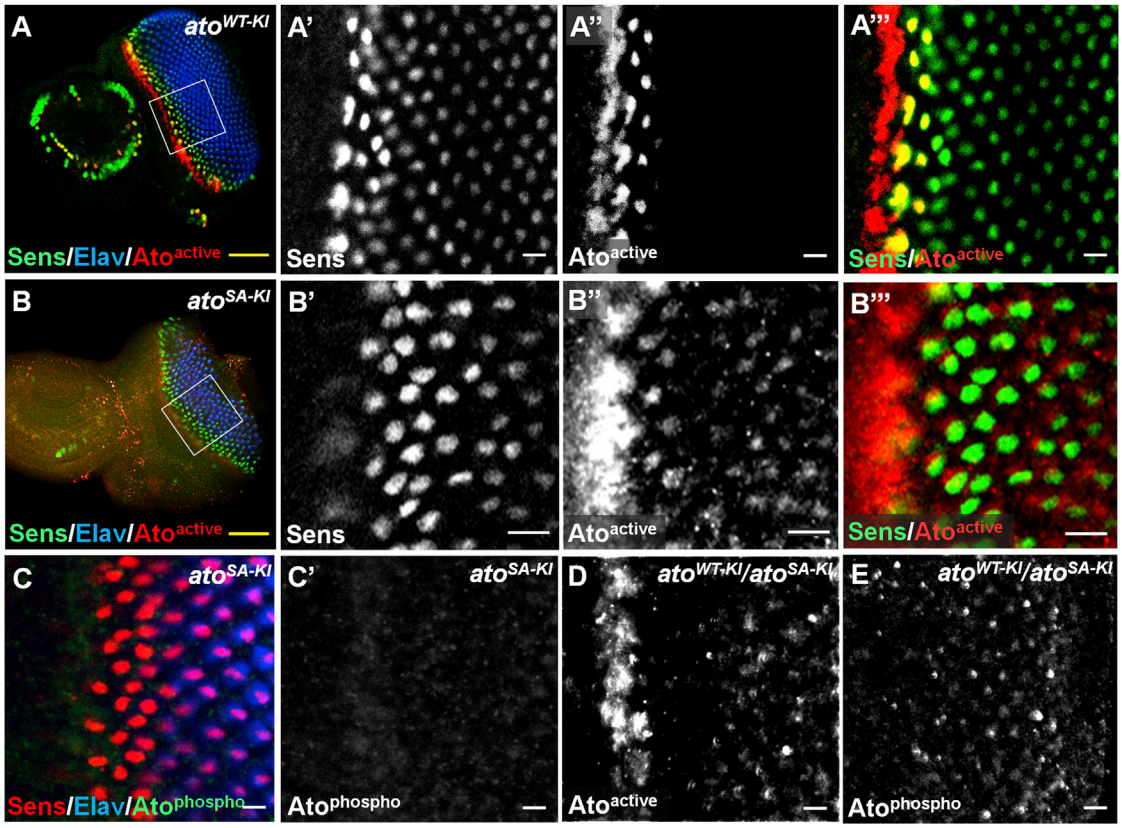

Figure 4. Loss of Ato Phosphorylation Alters Protein Dynamics

(A–A‴) Ato^{active} expression (red) in $ato^{WT\text{-}KI}$ eye discs also stained for Sens (green) and Elav (blue).

(B–B‴) Ato^{active} expression (red) in $ato^{SA\text{-}KI}$ L3 eye disc also stained for Sens (green) and Elav (blue).

(C and C′) $Ato^{phospho}$ expression (green) in $ato^{SA\text{-}KI}$ eye discs showing no detectable signal.

(D and E) $ato^{WT\text{-}KI}/ato^{SA\text{-}KI}$ L3 eye discs stained with αAto^{active} (D) and $\alpha Ato^{phospho}$ (E). In heterozygous eye discs, Ato^{active} and $Ato^{phospho}$ are both expressed posterior to the MF.

Scale bars, 50 μm in yellow and 10 μm in white. See also Figure S5.

mRNA (Figures S5A–S5B′). Even strong ectopic expression of Ato^{WT} and Ato^{SA} in the wing disc results in very weak to undetectable activation of the endogenous *ato* locus (Figures S5C–S5E′).

Altering Atonal Dynamics Inhibits Neurogenesis through Quantitative Dysregulation of Target Genes

If $Ato^{SA\text{-}KI}$ is a functional proneural protein, how does it cause the eye defects (Figure 3H) of $ato^{SA\text{-}KI}$ flies? We noted that $ato^{SA\text{-}KI}$ homozygous retinae contain some ommatidia of smaller size than others compared with the uniform size seen in controls (Figures 5A, 5C, S6A, and S6C). Quantification of the number of neurons per ommatidium reveals a distribution of cell numbers ranging from two to seven neurons per ommatidium, as opposed to the normal eight in controls (Figures 5H and 5I). The number of neurons is determined by a process of recruitment of surrounding cells by R8 into the ommatidial cluster via activation of EGFR signaling. Staining of $ato^{SA\text{-}KI}$ retina with antibodies to the double-phospho Mitogen Activated Protein Kinase (MAPK/dpERK) shows strong reduction in MAPK activation compared to controls (Figures S6E and S6F). These data suggest that EGFR signaling activity is compromised by the persistence of Ato protein expression. Consistent with this, heterozygosity for *egfr* in $ato^{SA\text{-}KI}$ flies results in strong further reduction of the dpERK signal (Figure S6G), and a strong reduction in the number of neurons per ommatidium (Figures 5B, 5D, 5H, 5I, S6B, and S6D) whereby 70% of ommatidia contain only the R8 cell (Figure 5I).

How does the persistence of Ato^{active} negatively regulate EGFR signaling upstream of MAPK? Ato may inappropriately elevate the expression of target genes that then negatively regulate EGFR activity. We first verified that the $ato^{SA\text{-}KI}$ activates all known Ato target enhancers in the retina in vivo, in contrast to $ato^{SD\text{-}KI}$ (Figure S4). We have previously identified several direct target genes of Ato (Aerts et al., 2010) including the cell adhesion molecule Fasciclin 2 (Fas2), whereby Ato upregulates Fas2 expression within the furrow (Aerts et al., 2010). Fas2 expression is then downregulated, but not lost, posterior to the furrow (Mao and Freeman, 2009) coincident with Ato inactivation. Fas2 is described as a quantitative inhibitor of EGFR activity during retinal development (Mao and Freeman, 2009). We find Fas2 to be increased in several differentiating photoreceptors of $ato^{SA\text{-}KI}$

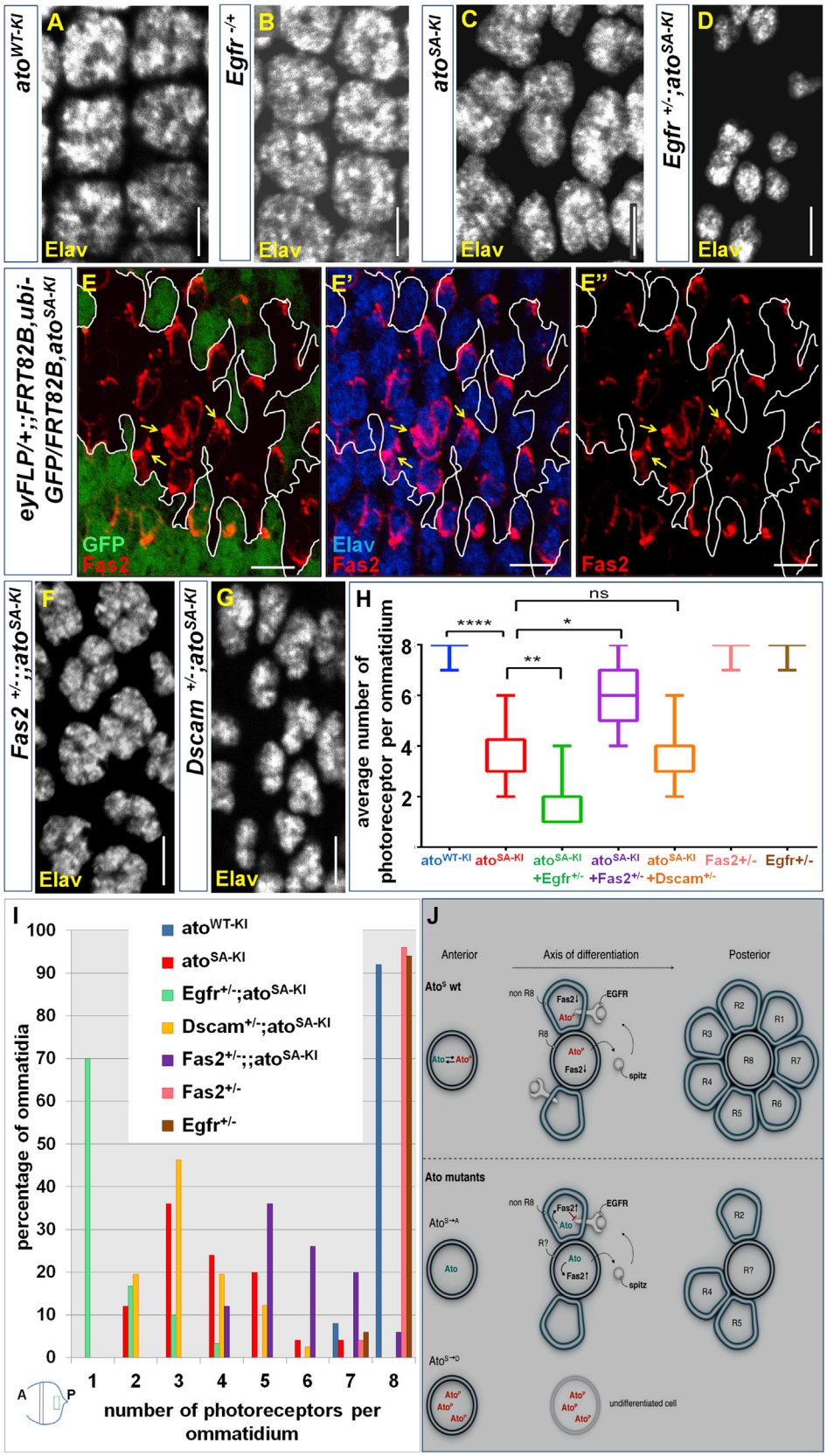

(legend on next page)

clones compared to surrounding control tissue (Figures 5E–5E″). Consistent with this, heterozygosity for a null allele of *fas2* in the $ato^{SA\text{-}KI}$ background results in a significant rescue of dpERK activation (Figure S6H) and photoreceptor numbers (Figure 5I) including a few ommatidia with the full complement of eight neurons (Figures 5H and 5I). In contrast, reducing the function of *Dscam*, also a cell adhesion molecule and target of Ato (Aerts et al., 2010), does not rescue $ato^{SA\text{-}KI}$ defects (Figures 5G–5I). Thus far, our data suggest a model whereby loss of phosphorylation results in abnormally prolonged proneural activity. Paradoxically, ectopic proneural activity results in inhibition of neuronal recruitment, at least in part, due to dysregulation of Ato target gene expression, such as Fas2, and the consequent interference with cellular signaling, including the EGFR pathway (Figure 5J).

Tampering with Atonal Activity Dynamics Alters Neuronal Fate

Timely inactivation of Ato by phosphorylation on S292 is essential for the proper quantitative regulation of target gene expression and the generation of the correct number of neurons. We asked whether the neurons that are generated in $ato^{SA\text{-}KI}$ animals are correctly specified. $ato^{SA\text{-}KI}$ retinae were examined for various fate markers. In wild-type and $ato^{WT\text{-}KI}$ control retinae, the R2/5 neurons express Rough (Ro), while R3/4 and R1/R6 express Seven-Up (Svp). Ro is initially expressed by R8 precursors as well, but is rapidly lost (Figures 6A and 6B) (Frankfort et al., 2001; Heberlein et al., 1991). Similarly, Sens and Svp expression are mutually exclusive (Figures 6A and 6D). In addition, each wild-type and control ommatidium contains a single Prospero (Pros) positive R7 neuron (Charlton-Perkins et al., 2011; Cook et al., 2003) (Figures 6A, 6F, 6G, 6L, and 6M). In $ato^{SA\text{-}KI}$ ommatidia, Ro expression is not downregulated in the differentiating R8, and ommatidia contain between one and three Ro positive cells (Figures 6C and 6J). Similarly, several R8s in the $ato^{SA\text{-}KI}$ retinae inappropriately express Svp and the number of Svp positive cells varies between ommatidia (Figures 6E and 6K). Finally, $ato^{SA\text{-}KI}$ retina show a variety of R7 defects including cells expressing both Sens and Pros (Figures 6H and 6L, arrows) and R7 duplications (yellow circle) and triplications (white circle) (Figures 6I and 6M). To test whether the temporal persistence of Ato expression is sufficient to cause cell-fate defects, the three forms of Ato (WT, SA, and SD) were misexpressed using either an anterior driver (*eyGal4*) or a posterior driver (*Gal4-7*) (Figures 6N–6S) and the cell-fate markers Sens (R8) and Svp (R3/4 and 1/6) examined. Expression of Ato^{WT} and Ato^{SA} induces cell-fate defects (white arrows) only when expressed late, but not only early (Figures 6N′–6Q′). Misexpression of Ato^{SD} caused no obvious defects in either case (Figures 6R′ and 6S′). Therefore, temporal dynamics of post-translational inactivation of Ato are essential for the proper specification of neuronal number and fate.

We explored the effects of $Ngn2^{WT}$, $Ngn2^{TA}$ and $Ngn2^{TD}$ in vivo on neuronal fate using in utero electroporation. $Ngn2^{WT}$ and $Ngn2^{TA}$ electroporated neurons displayed an identity of early born $Tbr1^{+}$ deep layer cortical neurons (Figure S7A), rather than later-born $Cux1^{+}$ upper-layer neurons (Figure S7B), a fate change that is consistent with precocious differentiation observed at early time point (E13.5–E14.5). In contrast, $Ngn2^{TD}$ produced a similar proportion of late-born $Cux1^{+}$ upper-layer neurons as in controls.

Phosphorylation Site Specificity Is Crucial for Activity Dynamics and Neuronal Fate

In vertebrates, the Ato-related Neurogenin (Ngn) proteins are required for the progenitor-to-neuron transition in a variety of lineages (Bertrand et al., 2002; Korzh and Strähle, 2002; Ma et al., 2008). Curiously, while Ato class proteins have an invariant Ser as the proneural phosphorylation site, Ngn proteins have an invariant Thr (Figure 7A). Although this is considered a very conservative substitution, it is intriguing that no known Ato protein contains a Thr at this position. We generated a Ser-to-Thr ($ato^{ST\text{-}KI}$) knockin fly. $ato^{ST\text{-}KI}$ flies are viable and fertile and show no obvious gross eye defects (Figures 7B and 7C), further confirming that this is a phosphorylation site. At the protein level, this change is predicted not to interfere with heterodimer formation, but to cause a slight, non-significant, increase (−0.29 kcal/mol) in DNA binding (Figures 7D–7G). Careful examination of Ato expression shows that active Ato (as detected by αAto^{active}) persists at low levels within the R8 for several rows (Figures 7H–7K). Examination of the eye disc with Sens and Elav shows no large-scale defects in neuronal fate. However, detailed examination shows that $ato^{ST\text{-}KI}$ ommatidia almost always contain two $Pros^{+}$ neurons instead of one (Figures 7L–7O‴).

DISCUSSION

We discovered a conserved post-translational switch regulating neurogenesis via the precise spatiotemporal control of proneural transcription factor activity. Using the fruit fly developing retina to dissect this mechanism, our data suggest a model whereby the proneural protein Ato is efficiently inactivated by phosphorylation of a single binary switch amino acid, creating a sharp spatial and temporal activity gradient. We are unable to detect any activity for phospho-mimetic forms of Ato and Ngn2 in proneural assays. However, we cannot completely rule out that the phospho forms have a function not related to DNA binding or proneural activity.

Figure 5. Loss of Ato Phosphorylation Reduces EGFR Signaling through Fas2

(A–D) High magnification of posterior areas of L3 eye discs stained for Elav. $ato^{WT\text{-}KI}$ (A), heterozygous *egfr[f2]*/+ (B), $ato^{SA\text{-}KI}$ (C), and *egfr[f2]*/+ (D); $ato^{SA\text{-}KI}$ eye discs. Homozygous $ato^{SA\text{-}KI}$ ommatidia show variable reduction in size (C). This is enhanced by heterozygosity for *egfr* (D).

(E–E‴) Homozygous $ato^{SA\text{-}KI}$ clones (GFP negative) stained for Elav and Fas2. $ato^{SA\text{-}KI}$ clones show increased Fas2 expression.

(F and G) High magnification of L3 eye discs stained for Elav. The $ato^{SA\text{-}KI}$ phenotype is suppressed by heterozygosity for *fas2* (F) but not *Dscam* (G).

(H) Quantification of the number of photoreceptors per ommatidium across the genotypes shown in (A)–(G). n = 50. *p < 0.01; **p < 0.007; ****p < 0.0001.

(I) Distribution of photoreceptor number per ommatidium, n = 50. Scale bar, 10 μm. See also Figure S6.

(J) Model for how dysregulation of Ato phosphorylation interferes with cellular signaling, including the EGFR pathway.

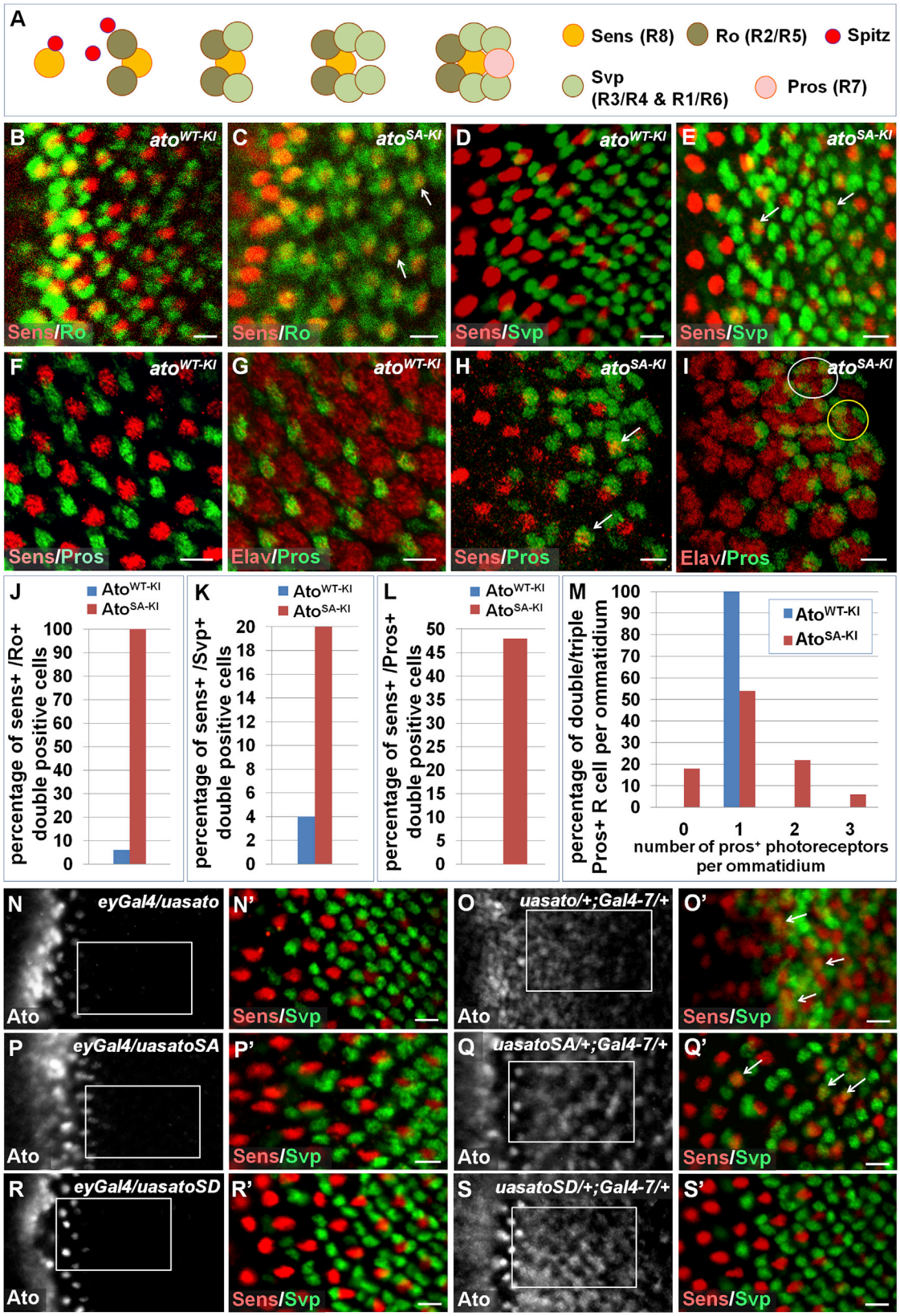

(legend on next page)

Several less conserved phosphorylation sites outside the bHLH domain of different proneural proteins have been identified (Ali et al., 2011; Hand et al., 2005; Li et al., 2012; Ma et al., 2008; Takebayashi et al., 1997; Yang et al., 2012). These sites have been proposed to alter proneural protein stability and interaction with putative partners, but very few have been directly tested at endogenous levels in vivo. Interestingly, based on biochemical analyses in vitro, it was proposed that phosphorylation of the proneural Ser in mouse Achaete-Scute homolog 1 (Mash1 S152) stabilizes it and increases Mash1/E47 heterodimer formation and consequently DNA binding and target gene activation (Viñals et al., 2004). Crucially, however, a phospho-mimetic form was not tested in that study, and effects on proneural activity were not assessed. In contrast, we show that phosphorylation inactivates proneural proteins and inhibits target gene expression. Although we analyzed Sc and not Mash1, we believe the discrepancy stems from the lack of analysis of phospho-mimetic isoforms of Mash1 and lack of in vivo analysis in the previous study, rather than a specific divergence of Mash1 compared to Sc, Ato, Atoh1, and Ngn2.

Our data suggest that all classes of proneural proteins are regulated by the phosphorylation of the exact same residue. The conservation of this effect is explained by the position of the Ser and Thr residues in the three-dimensional structure of the proneural heterodimer where it faces the phosphate groups of the DNA backbone. Phosphorylation of this residue creates repulsive electrostatic interactions with DNA increasing the energy required for DNA binding. This explains why the phospho-mimetic forms are essentially proneural-null mutants and how this modification acts as a binary switch. Interestingly, inhibiting an all-or-nothing proneural switch is translated into quantitative changes in target gene expression. Yet these relatively small changes in expression and cell-cell signaling are sufficient to cause strong defects in neuronal number and fate. Current models suggest that proneural proteins specify differential neuronal cell fate through on/off target gene expression. While this is clearly correct for many target genes, we find that subtle and quantitative spatiotemporal regulation is critical for proper neurogenesis.

Our data indicate that the same site on different proneural proteins may be phosphorylated by different kinases. For example, PKA is a regulator of Hedgehog signaling in the context of both retinal development in flies (Li et al., 1995) and the generation of mammalian cerebellar neurons (Niewiadomski et al., 2013), where Ato and Atoh1 are required, respectively. MARK1 is an autism candidate gene (Maussion et al., 2008), while PLK1 has recently been implicated in early neurogenesis of the mammalian cortex (Sakai et al., 2012). Therefore, the conserved proneural Ser/Thr residue is a potential target of phosphorylation by relevant context-specific kinases. One surprising finding is that, in vivo, change from Ser to Thr is not fully tolerated even though all known Ser kinases are also Thr Kinases. A potential explanation for this observation is the evidence that Ser/Thr kinases have a strong preference for Ser over Thr, while phosphatases appear to prefer Thr (Olsen et al., 2006; Pinna and Donella-Deana, 1994; Ubersax and Ferrell, 2007). These biases would predict that a change from a normal Ser to a Thr would result in less efficient phosphorylation and/or more efficient de-phosphorylation. Where phosphorylation deactivates the protein, as in the case of Ato, this would result in a shift of the equilibrium toward the active pool of the protein. The evidence from the $Ato^{ST\text{-}KI}$ mutant is consistent with these predictions.

Overall, our data indicate that we have identified a general mechanism for linking quantitative temporal dynamics of proneural protein activity to neural formation and diversification. We propose a working hypothesis whereby the precise spatial and temporal control of neurogenesis is regulated, at least in part, by the equilibrium between active and inactive pools of proneural proteins as cells transition from pluripotent progenitors to committed neuronal precursors. This post-translational equilibrium dictates the level and temporal dynamics of proneural activity to ensure that the subsequent steps of neuronal differentiation occur robustly.

Finally, coupling time and amplitude in transcription factor expression dynamics is a general phenomenon, although how it is achieved mechanistically has been unclear. An elegant example of this is provided by the role of the Sequoia protein during visual system wiring in *Drosophila* (Petrovic and Hummel, 2008). Sequoia levels increase and then decrease in the R8, only to then follow the same dynamics in the R7. The precision of these temporal amplitude changes is crucial for proper axonal wiring. In yeast, the Msn2 transcription factor that regulates glucose responses shows different temporal dynamics depending on environmental conditions. Recent work suggests that both the amplitude and frequency of Msn2 expression bursts

Figure 6. Ato Ser 292 to Ala Mutation Causes Cell-Fate Defects

(A) Scheme of sequential photoreceptor recruitment.

(B) Control $ato^{WT\text{-}KI}$ eye discs stained for Sens (red) and Ro (green) to mark R8 and R2/5 photoreceptors, respectively. After initial Ro expression in the R8, Sens, and Ro become mutually exclusive.

(C) $ato^{SA\text{-}KI}$ eye discs stained for Sens (R8; red) and Ro (R2/5; green). Many R8s continue to express Ro.

(D) Control $ato^{WT\text{-}KI}$ eye discs stained for Sens (red) and Svp (R3/4/1/6; green).

(E) $ato^{SA\text{-}KI}$ eye discs stained for Sens (red) and Svp (green). Many R8s express Svp.

(F and G) Control $ato^{WT\text{-}KI}$ eye discs stained for Sens (red) and Pros (R7; green) (F) or Pros (green) and Elav (red) (G). Sens and Pros are mutually exclusive and each ommatidium contains only one Pros positive neuron.

(H and I) $ato^{SA\text{-}KI}$ eye discs stained for Sens (red) and Pros (green) (H) or Pros (green) and Elav (red) (I). Many R8s express Pros (arrows) and many ommatidia contain two (yellow circle), or three (white circle), Pros positive neurons.

(J–M) Quantification of $Sens^+/Ro^+$ double-positive cells (J), $Sens^+/Svp^+$ double-positive cells (K), $Sens^+/Pros^+$ double-positive cells (L) and distribution of the number of ommatidia with multiple $Pros^+$ cells (M). n = 50. Scale bar, 10 μm.

(N–S′) Partial L3 eye disc stained for Sens and Svp upon mis-expression of Ato (N–O′), Ato^{SA} (P–Q′), Ato^{SD} (R–S′) with eyGal4 (N, P, and R) or Gal4-7 (O, Q, and S). Arrows indicate the Sens/Svp double-positive cells.

See also Figure S7.

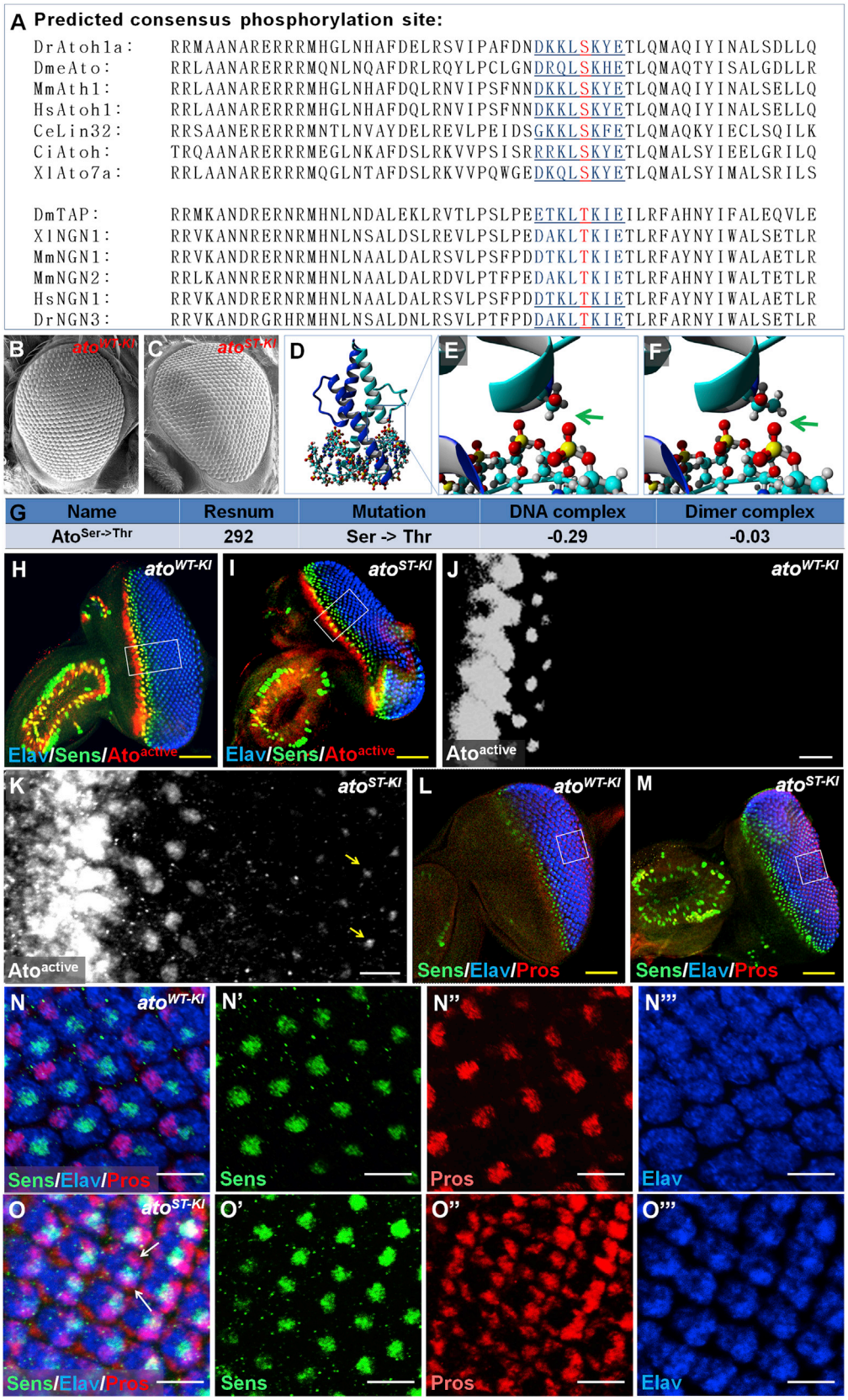

(legend on next page)

combine to transmit reliable environmental information to the yeast cell (Hansen and O'Shea, 2015). Here, we provide direct evidence that amplitude and time are coupled through post-translational modification of transcription factors and that this coupling is crucial for generating the correct number and diversity of cells. It would not surprise us if across phylogeny similar rules of protein activity control couple amplitude and duration in order to govern changes in cellular states.

EXPERIMENTAL PROCEDURES

Molecular Cloning, Fly Stocks, and Genetics

See Supplemental Experimental Procedures.

Immunohistochemistry

Immunohistochemistry on third-instar larval imaginal discs was performed as described (Mardon et al., 1994). Mouse embryos were fixed by perfusion with 4% paraformaldehyde. Immunofluorescence was performed on 100-μm sections. Primary antibodies were incubated overnight at 4°C and secondary during 2 hr at 15–25°C in PBS supplemented with 5% horse serum, 0.3% Triton X-100. Nuclei were stained with bisbenzimide (Hoechst#33258, Sigma). Sections were mounted with glycergel (DAKO). See Supplemental Experimental Procedures for antibody details.

In Situ Hybridization

In situ hybridization on eye imaginal discs was performed using standard protocols (Cubas et al., 1991).

In Vitro Kinase Assays

The peptide encompassing residues 286–300 of wild-type Ato or Ato^{SA} was phosphorylated by 0.5 U of PKA (Sigma P2645) in 25 mM Tris/HCl (pH 7.5), 0.1 mM [γ-^{32}P]ATP, and 2 mM magnesium acetate for 1 hr at 30°C. Reactions were stopped by transfer to P81 papers and washing with 75 mM orthophosphoric acid. Radioactivity was used as a measure of incorporated phosphate using a liquid scintillation counter. For the commercial kinase screen, see Supplemental Experimental Procedures.

Protein Immunoprecipitation

Ngn2 immunoprecipitation was performed as described (Tiberi et al., 2012) on dissected E14.5 cerebral cortices with anti-Ngn2 antibody (Santa Cruz Biotechnology, sc-19233) for endogenous Ngn2 and anti-myc antibody (Cell Signaling Technology, #2276) for exogenous Ngn2 WT-myc (WT) and Ngn2 T-A-myc (T-A). Where indicated, 400 units λ-phosphatase (NEB) was incubated with the sample at 30°C for 30 min. Antibody used for the western blot: anti-Ngn2 (Santa Cruz, sc-19233, anti-myc (Cell Signal, #2278), anti-phospo-Thr (Cell Signal, #9381).

Scanning Electron Microscopy of *Drosophila* Adult Eye

See Supplemental Experimental Procedures.

Yeast Two-Hybrid Assay

The yeast two-hybrid assay was performed by Hybrigenics as described in Supplemental Experimental Procedures.

Dual Luciferase Assay

Daoy cells (ATCC) were transfected using Lipofectamine LTX and Plus reagent (Invitrogen) per manufacturer's instructions. For each sample (1.25×10^5 cells), 200 ng of AtAEM firefly reporter, 40 ng of Renilla control, 250 ng of Atoh1 construct, and 250 ng of E47 construct were co-transfected. After 24 hr, cells were lysed and subjected to the dual luciferase reporter assay (Promega). Each experiment was repeated six times.

DNA Pull-Down Assay

Daoy cells (ATCC) were transfected using Lipofectamine LTX and Plus reagent (Invitrogen). 250 ng of Atoh1-GFP or Ngn2-Myc constructs were co-transfected with 250 ng of and E47-Flag constructs. After 24 hr, cells are lysed (50 mM Tris-Cl [pH 7.5], 150 mM NaCl, 1 mM EDTA, 0.5% Triton X-100 + protease and phosphatase inhibitors). Double-stranded DNA oligonucleotides were generated by synthesis of two biotinylated DNA oligos containing three times AtEAM sequence, mixing in a 1:1 ratio, denaturing for 5 min in boiling water and cooled over the course of 3 hr to room temperature, and finally diluting to a 10 μM stock. 20 pmol of oligonucleotides are conjugated to 15 μl agarose bead slurry for 30 min at 4°C and washed two times with lysis buffer before use. Each sample lysate is pre-cleared for 30 min with agarose beads and then incubated with 15 μl pre-conjugated agarose bead slurry for 2 hr at 4°C. Beads are washed three times with wash buffer (50 mM Tris-Cl [pH 7.5], 150 mM NaCl, 1 mM $MgCl_2$, 0.1% Triton X-100). Protein is eluted by adding NuPAGE LDS sample buffer (Invitrogen) to the beads and incubated in boiling water for 10 min.

GFP Immunoprecipitation

Daoy cells (ATCC) were transfected using Lipofectamine LTX and Plus reagent (Invitrogen) per manufacturer's instructions. For each sample (2.5×10^5 cells), 250 ng of Atoh1-GFP and E47-Flag constructs were transfected. 24 hr post-transfection, Daoy cells are lysed in mild lysis buffer (50 mM Tris-Cl [pH 7.5], 150 mM NaCl, 1 mM EDTA, 0.5% Triton X-100) supplemented with protease and phosphatase inhibitors. Lysates are pre-cleared for 30 min with agarose beads then added to GFP Trap beads (Chromotek) for 2 hr. Beads are washed three times with wash buffer (50 mM Tris-Cl [pH 7.5], 150 mM NaCl, 1 mM $MgCl_2$, 0.1% Triton X-100). Protein is eluted by adding NuPAGE LDS sample buffer (Invitrogen) to the beads and incubated in boiling water for 10 min.

Structural Modeling

See Supplemental Experimental Procedures.

Mouse In Utero Electroporation and Statistical Analysis

All mouse experiments were performed with the approval of the Université Libre de Bruxelles Committee for animal welfare. Briefly, timed pregnant CD1 mice at E13.5 were anesthetized, and their uterus was exposed. A solution of pCIG, pCIG Ngn2-myc, pCIG Ngn2(TA)-myc, and pCIG Ngn2(TD)-myc

Figure 7. Specificity of the Ato Group Proneural Ser

(A) Comparison of the proneural phosphorylation site between Ato and Ngn proteins. Ngn proteins always bear a Thr at the equivalent position to the Ato Ser.
(B and C) SEM image of adult eyes from $ato^{WT\text{-}KI}$ (B) and $ato^{ST\text{-}KI}$ animals (C).
(D) 3D model of Ato as heterodimer with Da bound to DNA.
(E and F) Close-up view of the Ser (E) or Thr (F).
(G) Predicted effects of the Ato Ser > Thr substitution on the energy of DNA binding and Ato/Da heterodimer formation.
(H and I) L3 eye discs from $ato^{WT\text{-}KI}$ (H) and $ato^{ST\text{-}KI}$ (I) animals stained for Ato^{active} (red), Sens (green), and Elav (blue). No large-scale abnormalities are visible at low magnification.
(J and K) High-magnification images showing details of the expression pattern of the Ato^{active} protein in $ato^{WT\text{-}KI}$ and $ato^{ST\text{-}KI}$ eye discs. Note low-level persistence of Ato^{ST} posterior to the MF.
(L and M) L3 eye discs from $ato^{WT\text{-}KI}$ (L) and $ato^{ST\text{-}KI}$ (M) animals stained for Pros (red), Sens (green), and Elav (blue). No large-scale abnormalities are visible at low magnification.
(N–O‴) High-magnification images of the discs shown in (L) and (M), respectively. While $ato^{WT\text{-}KI}$ discs (N–N‴) show a normal pattern of single Pros positive neuron per ommatidium, $ato^{ST\text{-}KI}$ ommatidia (O–O‴) show two Pros positive neurons per ommatidium (arrow). Scale bars, 50 μm in yellow and 10 μm in white.

(total concentration of 1 μg/μl) was injected into one lateral ventricle of in utero embryos and five to eight electric pulses at 30 V at E13.5, were delivered using forceps-type electrodes. Unless stated otherwise, data are presented as mean ± SD of at least three biologically independent in vivo experiments (three different litters), of four to six embryos. For quantification of cell numbers in vivo, at least 100 cells (for each embryo) were counted at similar rostrocaudal levels between animals. Whenever possible, quantifications were performed blind to condition, and no animals or data points were excluded during the analysis. One-sided Student's t test was used for calculating significance values.

SUPPLEMENTAL INFORMATION

Supplemental Information includes Supplemental Experimental Procedures, seven figures, and two tables and can be found with this article online at http://dx.doi.org/10.1016/j.cell.2015.12.048.

AUTHOR CONTRIBUTIONS

X.J.Q. designed the project, collected and analyzed data, made figures, and wrote the manuscript; L.T. collected and analyzed data, made figures, and wrote the manuscript; L.Y., N.D.G., A.C., J.Y., R.v.d.K., W.R.X., T.J.K., M. Bollen, and M. Beullens collected and analyzed data; P.V., J.S., F.R., H.Y.Z., M. Bollen, and M. Beullens analyzed data and commented on manuscript; and B.A.H. designed and supervised the project, analyzed data, wrote the manuscript.

ACKNOWLEDGMENTS

We are grateful to P. Callaerts, S. Aerts, M. Freeman, H. Bellen, J. Kiger, F. Guillemot, and the *Drosophila* Stock Center for flies, constructs, and antibodies. We thank F. Velez for technical assistance, members of B.A.H.'s lab for helpful discussions, and D. Schmucker, G. Halder, and P. Verstreken for comments on the manuscript. This work was supported by VIB, the WiBrain Interuniversity Attraction Pole network (Belspo; to B.A.H. and P.V.), the Funds for Scientific Research Flanders (Fonds Wetenschappelijke Onderzoeks; FWO) grants G.0543.08, G.0680.10, G.0681.10, and G.0503.12 (to B.A.H.), and a Flemish Concerted Research Action (GOA 10/18) grant (to M. Bollen and M. Beullens). L.Y. is a China Scholarship Council doctoral fellow. W.R.X. and T.J.K. are supported by a grant from the Cancer Prevention and Research Institute of Texas (CPRIT, RP110390). H.Y.Z. is a Howard Hughes Medical Institute investigator. The Switch Laboratory is supported by VIB, University of Leuven, the Funds for Scientific Research Flanders (Fonds Wetenschappelijke Onderzoeks; FWO), the Flanders Institute for Science and Technology (IWT), and the Federal Office for Scientific Affairs of Belgium (Belspo), IUAP P7/16. R.v.d.K. was supported by Boehringer Ingelheim Pharma GmbH and Co. KG. Work in the P.V.'s lab is funded by the Fond Nationale de Recherche Scientifique (FNRS), the Queen Elizabeth Medical Foundation, the WELBIO Program of the Walloon Region, the Fondation de Spoelbergh, the AXA Research Fund, and Fondation ULB.

Received: April 13, 2015
Revised: October 12, 2015
Accepted: December 22, 2015
Published: January 28, 2016

REFERENCES

Aerts, S., Quan, X.J., Claeys, A., Naval Sanchez, M., Tate, P., Yan, J., and Hassan, B.A. (2010). Robust target gene discovery through transcriptome perturbations and genome-wide enhancer predictions in Drosophila uncovers a regulatory basis for sensory specification. PLoS Biol. *8*, e1000435.

Ali, F., Hindley, C., McDowell, G., Deibler, R., Jones, A., Kirschner, M., Guillemot, F., and Philpott, A. (2011). Cell cycle-regulated multi-site phosphorylation of Neurogenin 2 coordinates cell cycling with differentiation during neurogenesis. Development *138*, 4267–4277.

Ben-Arie, N., Bellen, H.J., Armstrong, D.L., McCall, A.E., Gordadze, P.R., Guo, Q., Matzuk, M.M., and Zoghbi, H.Y. (1997). Math1 is essential for genesis of cerebellar granule neurons. Nature *390*, 169–172.

Bertrand, N., Castro, D.S., and Guillemot, F. (2002). Proneural genes and the specification of neural cell types. Nat. Rev. Neurosci. *3*, 517–530.

Brown, N.L., Kanekar, S., Vetter, M.L., Tucker, P.K., Gemza, D.L., and Glaser, T. (1998). Math5 encodes a murine basic helix-loop-helix transcription factor expressed during early stages of retinal neurogenesis. Development *125*, 4821–4833.

Campuzano, S., and Modolell, J. (1992). Patterning of the Drosophila nervous system: the achaete-scute gene complex. Trends Genet. *8*, 202–208.

Casarosa, S., Fode, C., and Guillemot, F. (1999). Mash1 regulates neurogenesis in the ventral telencephalon. Development *126*, 525–534.

Charlton-Perkins, M., Whitaker, S.L., Fei, Y., Xie, B., Li-Kroeger, D., Gebelein, B., and Cook, T. (2011). Prospero and Pax2 combinatorially control neural cell fate decisions by modulating Ras- and Notch-dependent signaling. Neural Dev. *6*, 20.

Choi, C.M., Vilain, S., Langen, M., Van Kelst, S., De Geest, N., Yan, J., Verstreken, P., and Hassan, B.A. (2009). Conditional mutagenesis in Drosophila. Science *324*, 54.

Cook, T., Pichaud, F., Sonneville, R., Papatsenko, D., and Desplan, C. (2003). Distinction between color photoreceptor cell fates is controlled by Prospero in Drosophila. Dev. Cell *4*, 853–864.

Cubas, P., de Celis, J.F., Campuzano, S., and Modolell, J. (1991). Proneural clusters of achaete-scute expression and the generation of sensory organs in the Drosophila imaginal wing disc. Genes Dev. *5*, 996–1008.

Fode, C., Gradwohl, G., Morin, X., Dierich, A., LeMeur, M., Goridis, C., and Guillemot, F. (1998). The bHLH protein NEUROGENIN 2 is a determination factor for epibranchial placode-derived sensory neurons. Neuron *20*, 483–494.

Frankfort, B.J., Nolo, R., Zhang, Z., Bellen, H., and Mardon, G. (2001). senseless repression of rough is required for R8 photoreceptor differentiation in the developing Drosophila eye. Neuron *32*, 403–414.

Freeman, M. (1994). The spitz gene is required for photoreceptor determination in the Drosophila eye where it interacts with the EGF receptor. Mech. Dev. *48*, 25–33.

Ghysen, A., and Dambly-Chaudiere, C. (1989). Genesis of the Drosophila peripheral nervous system. Trends Genet. *5*, 251–255.

Hand, R., Bortone, D., Mattar, P., Nguyen, L., Heng, J.I., Guerrier, S., Boutt, E., Peters, E., Barnes, A.P., Parras, C., et al. (2005). Phosphorylation of Neurogenin2 specifies the migration properties and the dendritic morphology of pyramidal neurons in the neocortex. Neuron *48*, 45–62.

Hansen, A.S., and O'Shea, E.K. (2015). Limits on information transduction through amplitude and frequency regulation of transcription factor activity. eLife *4*, e06559.

Hassan, B.A., and Bellen, H.J. (2000). Doing the MATH: is the mouse a good model for fly development? Genes Dev. *14*, 1852–1865.

Hassan, B.A., Bermingham, N.A., He, Y., Sun, Y., Jan, Y.N., Zoghbi, H.Y., and Bellen, H.J. (2000). atonal regulates neurite arborization but does not act as a proneural gene in the Drosophila brain. Neuron *25*, 549–561.

Heberlein, U., Mlodzik, M., and Rubin, G.M. (1991). Cell-fate determination in the developing Drosophila eye: role of the rough gene. Development *112*, 703–712.

Jan, Y.N., and Jan, L.Y. (1994). Neuronal cell fate specification in Drosophila. Curr. Opin. Neurobiol. *4*, 8–13.

Jarman, A.P., Grau, Y., Jan, L.Y., and Jan, Y.N. (1993). atonal is a proneural gene that directs chordotonal organ formation in the Drosophila peripheral nervous system. Cell *73*, 1307–1321.

Jarman, A.P., Grell, E.H., Ackerman, L., Jan, L.Y., and Jan, Y.N. (1994). Atonal is the proneural gene for Drosophila photoreceptors. Nature *369*, 398–400.

Jarman, A.P., Sun, Y., Jan, L.Y., and Jan, Y.N. (1995). Role of the proneural gene, atonal, in formation of Drosophila chordotonal organs and photoreceptors. Development *121*, 2019–2030.

Klisch, T.J., Xi, Y., Flora, A., Wang, L., Li, W., and Zoghbi, H.Y. (2011). In vivo Atoh1 targetome reveals how a proneural transcription factor regulates cerebellar development. Proc. Natl. Acad. Sci. USA *108*, 3288–3293.

Korzh, V., and Strähle, U. (2002). Proneural, prosensory, antiglial: the many faces of neurogenins. Trends Neurosci. *25*, 603–605.

Krieger, E., and Vriend, G. (2002). Models@Home: distributed computing in bioinformatics using a screensaver based approach. Bioinformatics *18*, 315–318.

Krieger, E., Koraimann, G., and Vriend, G. (2002). Increasing the precision of comparative models with YASARA NOVA–a self-parameterizing force field. Proteins *47*, 393–402.

Kumar, J.P. (2010). Retinal determination the beginning of eye development. Curr. Top. Dev. Biol. *93*, 1–28.

Li, W., Ohlmeyer, J.T., Lane, M.E., and Kalderon, D. (1995). Function of protein kinase A in hedgehog signal transduction and Drosophila imaginal disc development. Cell *80*, 553–562.

Li, S., Mattar, P., Zinyk, D., Singh, K., Chaturvedi, C.P., Kovach, C., Dixit, R., Kurrasch, D.M., Ma, Y.C., Chan, J.A., et al. (2012). GSK3 temporally regulates neurogenin 2 proneural activity in the neocortex. J. Neurosci. *32*, 7791–7805.

Ma, Q., Chen, Z., del Barco Barrantes, I., de la Pompa, J.L., and Anderson, D.J. (1998). neurogenin1 is essential for the determination of neuronal precursors for proximal cranial sensory ganglia. Neuron *20*, 469–482.

Ma, Y.C., Song, M.R., Park, J.P., Henry Ho, H.Y., Hu, L., Kurtev, M.V., Zieg, J., Ma, Q., Pfaff, S.L., and Greenberg, M.E. (2008). Regulation of motor neuron specification by phosphorylation of neurogenin 2. Neuron *58*, 65–77.

Mao, Y., and Freeman, M. (2009). Fasciclin 2, the Drosophila orthologue of neural cell-adhesion molecule, inhibits EGF receptor signalling. Development *136*, 473–481.

Mardon, G., Solomon, N.M., and Rubin, G.M. (1994). dachshund encodes a nuclear protein required for normal eye and leg development in Drosophila. Development *120*, 3473–3486.

Maussion, G., Carayol, J., Lepagnol-Bestel, A.M., Tores, F., Loe-Mie, Y., Milbreta, U., Rousseau, F., Fontaine, K., Renaud, J., Moalic, J.M., et al. (2008). Convergent evidence identifying MAP/microtubule affinity-regulating kinase 1 (MARK1) as a susceptibility gene for autism. Hum. Mol. Genet. *17*, 2541–2551.

Nieto, M., Schuurmans, C., Britz, O., and Guillemot, F. (2001). Neural bHLH genes control the neuronal versus glial fate decision in cortical progenitors. Neuron *29*, 401–413.

Niewiadomski, P., Zhujiang, A., Youssef, M., and Waschek, J.A. (2013). Interaction of PACAP with Sonic hedgehog reveals complex regulation of the hedgehog pathway by PKA. Cell. Signal. *25*, 2222–2230.

Nolo, R., Abbott, L.A., and Bellen, H.J. (2001). Drosophila Lyra mutations are gain-of-function mutations of senseless. Genetics *157*, 307–315.

Olsen, J.V., Blagoev, B., Gnad, F., Macek, B., Kumar, C., Mortensen, P., and Mann, M. (2006). Global, in vivo, and site-specific phosphorylation dynamics in signaling networks. Cell *127*, 635–648.

Petrovic, M., and Hummel, T. (2008). Temporal identity in axonal target layer recognition. Nature *456*, 800–803.

Pinna, L.A., and Donella-Deana, A. (1994). Phosphorylated synthetic peptides as tools for studying protein phosphatases. Biochim. Biophys. Acta *1222*, 415–431.

Quan, X.J., Denayer, T., Yan, J., Jafar-Nejad, H., Philippi, A., Lichtarge, O., Vleminckx, K., and Hassan, B.A. (2004). Evolution of neural precursor selection: functional divergence of proneural proteins. Development *131*, 1679–1689.

Quan, X.J., Ramaekers, A., and Hassan, B.A. (2012). Transcriptional control of cell fate specification: lessons from the fly retina. Curr. Top. Dev. Biol. *98*, 259–276.

Rister, J., Desplan, C., and Vasiliauskas, D. (2013). Establishing and maintaining gene expression patterns: insights from sensory receptor patterning. Development *140*, 493–503.

Sakai, D., Dixon, J., Dixon, M.J., and Trainor, P.A. (2012). Mammalian neurogenesis requires Treacle-Plk1 for precise control of spindle orientation, mitotic progression, and maintenance of neural progenitor cells. PLoS Genet. *8*, e1002566.

Schymkowitz, J., Borg, J., Stricher, F., Nys, R., Rousseau, F., and Serrano, L. (2005). The FoldX web server: an online force field. Nucleic Acids Res. *33*, W382–W388.

Takebayashi, K., Takahashi, S., Yokota, C., Tsuda, H., Nakanishi, S., Asashima, M., and Kageyama, R. (1997). Conversion of ectoderm into a neural fate by ATH-3, a vertebrate basic helix-loop-helix gene homologous to Drosophila proneural gene atonal. EMBO J. *16*, 384–395.

Tiberi, L., Vanderhaeghen, P., and van den Ameele, J. (2012). Cortical neurogenesis and morphogens: diversity of cues, sources and functions. Curr. Opin. Cell Biol. *24*, 269–276.

Tio, M., Ma, C., and Moses, K. (1994). spitz, a Drosophila homolog of transforming growth factor-alpha, is required in the founding photoreceptor cells of the compound eye facets. Mech. Dev. *48*, 13–23.

Ubersax, J.A., and Ferrell, J.E., Jr. (2007). Mechanisms of specificity in protein phosphorylation. Nat. Rev. Mol. Cell Biol. *8*, 530–541.

Viñals, F., Reiriz, J., Ambrosio, S., Bartrons, R., Rosa, J.L., and Ventura, F. (2004). BMP-2 decreases Mash1 stability by increasing Id1 expression. EMBO J. *23*, 3527–3537.

Wang, S.W., Kim, B.S., Ding, K., Wang, H., Sun, D., Johnson, R.L., Klein, W.H., and Gan, L. (2001). Requirement for math5 in the development of retinal ganglion cells. Genes Dev. *15*, 24–29.

Wang, V.Y., Hassan, B.A., Bellen, H.J., and Zoghbi, H.Y. (2002). Drosophila atonal fully rescues the phenotype of Math1 null mice: new functions evolve in new cellular contexts. Curr. Biol. *12*, 1611–1616.

Wolff, T., and Ready, D.F. (1991). The beginning of pattern formation in the Drosophila compound eye: the morphogenetic furrow and the second mitotic wave. Development *113*, 841–850.

Yang, M., Hatton-Ellis, E., and Simpson, P. (2012). The kinase Sgg modulates temporal development of macrochaetes in Drosophila by phosphorylation of Scute and Pannier. Development *139*, 325–334.

Zhao, H., Ayrault, O., Zindy, F., Kim, J.H., and Roussel, M.F. (2008). Post-transcriptional down-regulation of Atoh1/Math1 by bone morphogenic proteins suppresses medulloblastoma development. Genes Dev. *22*, 722–727.